

Ultraviolet completion of pseudo-Nambu-Goldstone dark matter with a hidden U(1) gauge symmetry

Dan-Yang Liu, Chengfeng Cai, Xue-Min Jiang, Zhao-Huan Yu,^{*} and Hong-Hao Zhang[†]

School of Physics, Sun Yat-Sen University, Guangzhou 510275, China

We propose an ultraviolet completion model for pseudo-Nambu-Goldstone dark matter with a hidden U(1) gauge symmetry. Compared to previous studies, this setup is simpler, introducing less interactions. Dark matter scattering off nucleons is highly suppressed by the ultraviolet scale and direct detection constraints can be easily evaded. The kinetic mixing between the hidden U(1) and the U(1)_Y gauge fields would lead to dark matter decays. We find that the current bound on the dark matter lifetime implies that the ultraviolet scale should be higher than 10^{10} GeV. The phenomenological constraints from the 125 GeV Higgs measurements, the dark matter relic density, and indirect detection of dark matter annihilation are also investigated.

CONTENTS

I. Introduction	2
II. Model	3
A. Lagrangian	3
B. Interactions	6
III. Phenomenology	9
A. WIMP-nucleon Scattering	10
B. WIMP Lifetime	11
C. Higgs Physics	13
D. WIMP Annihilation	14
IV. Parameter Scan	15
V. Conclusions and Discussions	18
Acknowledgments	18
References	19

^{*} Corresponding author. yuzhaoh5@mail.sysu.edu.cn

[†] Corresponding author. zh98@mail.sysu.edu.cn

I. INTRODUCTION

The cosmological abundance of dark matter (DM) can be naturally explained by neutral weakly interacting massive particles (WIMPs) which are thermally produced in the plasma and subsequently freeze out as the Universe expands [1–3]. The crucial ingredient in this argument is the weak interaction strength of WIMP annihilation into standard model (SM) particles at the freeze-out epoch, implying that WIMP dark matter is quite promising to be probed in current direct detection experiments. Although the direct detection sensitivity has been tremendously improved in the recent two decades, no robust signal has been found, suggesting severe constraints on the WIMP-nucleon scattering cross section [4, 5]. This situation makes the WIMP paradigm questionable.

Nonetheless, an annihilation cross section of weak strength does not necessarily result in a WIMP-nucleon scattering cross section of the same strength. It is possible to greatly suppress the scattering process in direct detection without affecting the annihilation processes at the freeze-out epoch. An elegant way to realize it is to assume that the WIMP is a pseudo-Nambu-Goldstone boson (pNGB) whose interactions are momentum-suppressed [6–32]. Since direct detection experiments basically operate at zero momentum transfer, the WIMP-nucleon scattering cross section totally vanishes at tree level [6], evading the direct detection constraints.

The original pNGB DM model [6] introduces a complex scalar S , which is a SM gauge singlet. The Lagrangian respects a $U(1)$ global symmetry $S \rightarrow e^{i\alpha}S$, except for a quadratic term $\mu_S^2(S^2 + S^{\dagger 2})/4$, which softly breaks the $U(1)$ symmetry into a Z_2 symmetry. After the $U(1)$ spontaneous breaking, the imaginary part of S becomes a stable pNGB, which has a mass μ'_S and acts as the WIMP with a vanishing tree-level WIMP-nucleon scattering amplitude. Such a soft breaking term is *ad hoc*. Other soft breaking terms, such as a trilinear term $\propto S^3 + S^{\dagger 3}$, would spoil the vanishing scattering amplitude. Therefore, it demands an appropriate ultraviolet (UV) completion to realize only this quadratic soft breaking term [6].

A possible UV completion is to gauge the $U(1)$ symmetry with $B - L$ charges [17, 18]. Such a $U(1)_{B-L}$ gauge symmetry would be free from gauge anomalies if three right-handed neutrinos are introduced. Consequently, the WIMP-nucleon amplitude would not exactly vanish at tree level, but be suppressed by a UV scale, i.e., the breaking scale of the $U(1)_{B-L}$ gauge symmetry. In addition, the pNGB WIMP becomes unstable, and the constraint on its lifetime leads to a UV scale typically exceeding $\mathcal{O}(10^{11}-10^{13})$ GeV [17, 18]. Such a high scale UV completion can be embedded into a grand unified theory [22, 23].

In this work, we would like to decrease the UV scale, because a lower scale may be easier to be probed in future indirect detection and collider experiments. For this purpose, we assume the pNGB WIMP arising from a *hidden* $U(1)_X$ gauge symmetry, where all the SM fields do not carry $U(1)_X$ charges. The gauge anomalies are canceled without introducing right-handed neutrinos, so less fields are involved in this setup. Since the $U(1)_X$ gauge boson does not couple to SM fermions via any $U(1)_X$ gauge interaction, the interactions inducing WIMP decays only come from the kinetic mixing between the $U(1)_X$ and $U(1)_Y$ gauge fields, relieving the lifetime constraint on the UV scale.

This paper is organized as follows. In Section II, we construct a UV-complete model for pNGB WIMP by extending the SM by a hidden $U(1)_X$ gauge symmetry and two $U(1)_X$ -charged scalar fields. In Section III, we discuss the phenomenology of this model regarding the WIMP-nucleon scattering in direct detection experiments, the WIMP lifetime, the related Higgs physics, and the WIMP annihilation relevant to the relic abundance and indirect detection experiments. Section IV presents results from a random scan in the parameter space. Section V gives a summary of the paper.

II. MODEL

We extend the SM with a $U(1)_X$ gauge symmetry accompanied with two complex scalar fields S and Φ , which are SM gauge singlets but carry $U(1)_X$ charges $q_S = 1$ and $q_\Phi = 2$, respectively. All the SM fields do not carry $U(1)_X$ charges. We assume that S and Φ develop nonzero vacuum expectation values (VEVs) v_S and v_Φ with a hierarchy $v_S \ll v_\Phi$. Thus, v_Φ represents a UV scale that breaks the $U(1)_X$ gauge symmetry into an approximate $U(1)_X$ global symmetry. Beneath the lower scale v_S , the $U(1)_X$ global symmetry is spontaneously broken, resulting in a pNGB WIMP.

A. Lagrangian

The $SU(2)_L \times U(1)_Y \times U(1)_X$ gauge-invariant Lagrangian involving S , Φ , the SM Higgs doublet H , the $U(1)_X$ gauge field X^μ , and the $U(1)_Y$ gauge field B^μ reads

$$\begin{aligned} \mathcal{L} \supset & (D^\mu H)^\dagger (D_\mu H) + (D^\mu S)^\dagger (D_\mu S) + (D^\mu \Phi)^\dagger (D_\mu \Phi) - \frac{1}{4} B^{\mu\nu} B_{\mu\nu} - \frac{1}{4} X^{\mu\nu} X_{\mu\nu} \\ & - \frac{s_\varepsilon}{2} B^{\mu\nu} X_{\mu\nu} + \mu_H^2 |H|^2 + \mu_S^2 |S|^2 + \mu_\Phi^2 |\Phi|^2 - \frac{\lambda_H}{2} |H|^4 - \frac{\lambda_S}{2} |S|^4 - \frac{\lambda_\Phi}{2} |\Phi|^4 \\ & - \lambda_{HS} |H|^2 |S|^2 - \lambda_{H\Phi} |H|^2 |\Phi|^2 - \lambda_{S\Phi} |S|^2 |\Phi|^2 + \frac{1}{\sqrt{2}} (\mu_{S\Phi} \Phi^\dagger S^2 + \text{H.c.}). \end{aligned} \quad (1)$$

The covariant derivatives of the scalars are $D_\mu H = (\partial_\mu - ig' B_\mu/2 - ig W_\mu^a \sigma^a/2)H$, $D_\mu S = (\partial_\mu - iq_S g_X X_\mu)S$, and $D_\mu \Phi = (\partial_\mu - iq_\Phi g_X X_\mu)\Phi$, where g_X denotes the $U(1)_X$ gauge coupling. The field strengths of B^μ and X^μ are defined as $B_{\mu\nu} \equiv \partial_\mu B_\nu - \partial_\nu B_\mu$ and $X_{\mu\nu} \equiv \partial_\mu X_\nu - \partial_\nu X_\mu$. The $B^{\mu\nu} X_{\mu\nu}$ term implies a kinetic mixing between B^μ and X^μ with a mixing parameter $s_\varepsilon \equiv \sin \varepsilon \in (-1, 1)$.

The parameter $\mu_{S\Phi}$ can be made real and positive by redefining the phase of S , and thus we adopt $\mu_{S\Phi} > 0$ hereafter. The scalar fields can be decomposed as

$$H = \frac{1}{\sqrt{2}} \begin{pmatrix} 0 \\ v + h \end{pmatrix}, \quad S = \frac{1}{\sqrt{2}} (v_S + s + i\eta_S), \quad \Phi = \frac{1}{\sqrt{2}} (v_\Phi + \phi + i\eta_\Phi), \quad (2)$$

where the SM Higgs field is expressed in the unitary gauge and $v = 246.22$ GeV. When mini-

mizing the scalar potential, three stationary point conditions are obtained as

$$\begin{aligned}\mu_H^2 &= \frac{1}{2}(\lambda_H v^2 + \lambda_{HS} v_S^2 + \lambda_{H\Phi} v_\Phi^2), \\ \mu_S^2 &= \frac{1}{2}(\lambda_S v_S^2 + \lambda_{HS} v^2 + \lambda_{S\Phi} v_\Phi^2) - \mu_{S\Phi} v_\Phi, \\ \mu_\Phi^2 &= \frac{1}{2}(\lambda_\Phi v_\Phi^2 + \lambda_{H\Phi} v^2 + \lambda_{S\Phi} v_S^2) - \frac{\mu_{S\Phi} v_S^2}{2v_\Phi}.\end{aligned}\quad (3)$$

The v_Φ contribution to the $\Phi^\dagger S^2$ term leads to

$$\mathcal{L}_{\text{soft}} = \frac{\mu_S'^2}{4}(S^2 + S^{\dagger 2}), \quad (4)$$

with $\mu_S'^2 = 2\mu_{S\Phi} v_\Phi$. This is the quadratic term directly introduced in the original pNGB DM model [6] to softly break the $U(1)_X$ global symmetry. In the limit $v_\Phi \rightarrow \infty$ and $\mu_{S\Phi} \rightarrow 0$ with finite $\mu_S'^2$, the original model is recovered. For a finite v_Φ , there should be some phenomenological deviations from the original model, which will be explored below.

After the scalar fields obtain the nonzero VEVs, the mass terms for the CP -even scalars (h, s, ϕ) and the CP -odd scalars (η_S, η_Φ) become

$$\mathcal{L}_{\text{mass}} \supset -\frac{1}{2} \begin{pmatrix} h & s & \phi \end{pmatrix} M_E^2 \begin{pmatrix} h \\ s \\ \phi \end{pmatrix} - \frac{1}{2} \begin{pmatrix} \eta_S & \eta_\Phi \end{pmatrix} M_O^2 \begin{pmatrix} \eta_S \\ \eta_\Phi \end{pmatrix}, \quad (5)$$

where the mass-squared matrices are given by [17]

$$M_E^2 = \begin{pmatrix} \lambda_H v^2 & \lambda_{HS} v v_S & \lambda_{H\Phi} v v_\Phi \\ \lambda_{HS} v v_S & \lambda_S v_S^2 & \lambda_{S\Phi} v_S v_\Phi - \mu_{S\Phi} v_S \\ \lambda_{H\Phi} v v_\Phi & \lambda_{S\Phi} v_S v_\Phi - \mu_{S\Phi} v_S & \lambda_\Phi v_\Phi^2 + \frac{\mu_{S\Phi} v_S^2}{2v_\Phi} \end{pmatrix}, \quad (6)$$

$$M_O^2 = \mu_{S\Phi} \begin{pmatrix} 2v_\Phi & -v_S \\ -v_S & \frac{v_S^2}{2v_\Phi} \end{pmatrix}. \quad (7)$$

The two matrices can be diagonalized by two real orthogonal matrices U and V :

$$U^T M_E^2 U = \text{diag}(m_{h_1}^2, m_{h_2}^2, m_{h_3}^2), \quad V^T M_O^2 V = \text{diag}(m_\chi^2, 0). \quad (8)$$

V can be explicitly expressed as

$$V = \begin{pmatrix} c_\beta & s_\beta \\ -s_\beta & c_\beta \end{pmatrix}, \quad (9)$$

with a rotation angle β satisfying

$$s_\beta = \frac{v_S}{\sqrt{v_S^2 + 4v_\Phi^2}}. \quad (10)$$

We have adopted the shorthand notations for the trigonometric functions, $s_\beta \equiv \sin \beta$, $c_\beta \equiv \cos \beta$, and $t_\beta \equiv \tan \beta$. Such notations are used throughout the paper.

The relations between the interaction and mass bases are

$$\begin{pmatrix} h \\ s \\ \phi \end{pmatrix} = U \begin{pmatrix} h_1 \\ h_2 \\ h_3 \end{pmatrix}, \quad \begin{pmatrix} \eta_S \\ \eta_\Phi \end{pmatrix} = V \begin{pmatrix} \chi \\ \tilde{\chi} \end{pmatrix}. \quad (11)$$

We define h_1 to be the SM-like Higgs boson with $m_{h_1} = 125.10 \pm 0.14$ GeV [33], whose dominant component should be h , i.e., $|U_{11}| > |U_{21}|, |U_{31}|$. Similarly, the exotic Higgs bosons h_2 and h_3 with masses m_{h_2} and m_{h_3} are defined as s -like and ϕ -like, respectively. We further use positive U_{11} , U_{22} , and U_{33} to fix the signs of the U matrix elements. $\tilde{\chi}$ is the massless Nambu-Goldstone boson associated with the spontaneous breaking of the $U(1)_X$ gauge symmetry, while χ is a pNGB WIMP with a mass squared of

$$m_\chi^2 = \frac{\mu_{S\Phi}}{2v_\Phi} (v_S^2 + 4v_\Phi^2), \quad (12)$$

serving as a DM candidate. The typical range for m_χ would be $\mathcal{O}(\text{GeV})$ – $\mathcal{O}(\text{TeV})$.

If $\mu_{S\Phi} = 0$, the Lagrangian (1) respects two distinct $U(1)$ global symmetries, one with $S \rightarrow e^{i\alpha_1} S$ and the other one with $\Phi \rightarrow e^{i\alpha_2} \Phi$. Consequently, both η_S and η_Φ are massless Nambu-Goldstone bosons according to the Goldstone theorem [34, 35]. Nonetheless, the existence of the $\mu_{S\Phi}$ term merges the two $U(1)$ symmetries into the $U(1)_X$ global symmetry with $q_S = 1$ and $q_\Phi = 2$. As a result, only $\tilde{\chi}$ remains massless, while χ obtains a mass proportional to $\sqrt{\mu_{S\Phi}}$.

After the spontaneous breaking of the $SU(2)_L \times U(1)_Y \times U(1)_X$ gauge symmetry, the gauge fields obtain the mass terms

$$\mathcal{L}_{\text{mass}} \supset m_W^2 W^{-,\mu} W_\mu^+ + \frac{1}{2} \begin{pmatrix} B^\mu & W^{3,\mu} & X^\mu \end{pmatrix} M_N^2 \begin{pmatrix} B_\mu \\ W_\mu^3 \\ X_\mu \end{pmatrix}, \quad (13)$$

with $m_W^2 = g^2 v^2 / 4$ and

$$M_N^2 = \begin{pmatrix} g^2 v^2 / 4 & -gg' v^2 / 4 & 0 \\ -gg' v^2 / 4 & g^2 v^2 / 4 & 0 \\ 0 & 0 & g_X^2 (v_S^2 + 4v_\Phi^2) \end{pmatrix}. \quad (14)$$

Considering both such a B_μ - W_μ^3 mass mixing and the B_μ - X_μ kinetic mixing, the physical neutral

gauge fields (A_μ, Z_μ, Z'_μ) can be obtained through a linear transformation [36, 37]

$$\begin{pmatrix} B_\mu \\ W_\mu^3 \\ X_\mu \end{pmatrix} = K \begin{pmatrix} A_\mu \\ Z_\mu \\ Z'_\mu \end{pmatrix} \quad (15)$$

with

$$K = \begin{pmatrix} \hat{c}_W & -\hat{s}_W c_\xi - t_\varepsilon s_\xi & \hat{s}_W s_\xi - t_\varepsilon c_\xi \\ \hat{s}_W & \hat{c}_W c_\xi & -\hat{c}_W s_\xi \\ 0 & s_\xi/c_\varepsilon & c_\xi/c_\varepsilon \end{pmatrix}. \quad (16)$$

Here we denote $\hat{s}_W \equiv \sin \hat{\theta}_W$ and $\hat{c}_W \equiv \cos \hat{\theta}_W$, where $\hat{\theta}_W \equiv \tan^{-1}(g'/g)$ is the weak mixing angle. ε is the angle related to the kinetic mixing, and ξ is a rotation angle determined by the equation [36]

$$t_{2\xi} = \frac{s_{2\varepsilon} \hat{s}_W v^2 (g^2 + g'^2)}{c_\varepsilon^2 v^2 (g^2 + g'^2) (1 - \hat{s}_W^2 t_\varepsilon^2) - 4g_X^2 (v_S^2 + 4v_\Phi^2)}. \quad (17)$$

The gauge fields (A_μ, Z_μ, Z'_μ) have canonical kinetic terms as well as diagonalized mass terms. The corresponding masses for the photon, Z , and Z' bosons are given by $m_A = 0$ and [38]

$$m_Z^2 = \frac{v^2}{4} (g^2 + g'^2) (1 + \hat{s}_W t_\varepsilon t_\xi), \quad m_{Z'}^2 = \frac{g_X^2 (v_S^2 + 4v_\Phi^2)}{c_\varepsilon^2 (1 + \hat{s}_W t_\varepsilon t_\xi)}, \quad (18)$$

respectively. Define $r \equiv m_{Z'}^2/m_Z^2$, and we can further derive [37]

$$t_\xi = \frac{2\hat{s}_W t_\varepsilon}{1-r} \left[1 + \sqrt{1-r \left(\frac{2\hat{s}_W t_\varepsilon}{1-r} \right)^2} \right]^{-1}. \quad (19)$$

$r \gg 1$ would lead to

$$t_\xi \simeq -\frac{\hat{s}_W t_\varepsilon}{r} + \mathcal{O}(r^{-2}). \quad (20)$$

If there is no kinetic mixing between B_μ and X_μ , we have $\varepsilon = \xi = 0$, $m_Z^2 = (g^2 + g'^2)v^2/4$, and $m_{Z'}^2 = g_X^2(v_S^2 + 4v_\Phi^2)$.

B. Interactions

In the basis of the mass eigenstates χ and h_i , the scalar trilinear couplings can be expressed as

$$\mathcal{L}_{\text{tri}} = -\frac{1}{2} \sum_{i=1}^3 g_{h_i \chi^2} h_i \chi^2 - \sum_{i,j,k=1}^3 g_{h_i h_j h_k} h_i h_j h_k, \quad (21)$$

where

$$g_{h_i\chi^2} = (\lambda_{HS}c_\beta^2 + \lambda_{H\Phi}s_\beta^2)vU_{1i} + (\lambda_S v_S c_\beta^2 + \lambda_{S\Phi} v_S s_\beta^2 + 2\mu_{S\Phi} s_\beta c_\beta)U_{2i} \\ + [\lambda_\Phi v_\Phi s_\beta^2 + (\lambda_{S\Phi} v_\Phi + \mu_{S\Phi})c_\beta^2]U_{3i}, \quad (22)$$

$$g_{h_i h_j h_k} = \frac{1}{2}(\lambda_H v U_{1i} + \lambda_{HS} v_S U_{2i} + \lambda_{H\Phi} v_\Phi U_{3i})U_{1j}U_{1k} \\ + \frac{1}{2}[\lambda_{HS} v U_{1i} + \lambda_S v_S U_{2i} + (\lambda_{S\Phi} v_\Phi - \mu_{S\Phi})U_{3i}]U_{2j}U_{2k} \\ + \frac{1}{2}(\lambda_{H\Phi} v U_{1i} + \lambda_{S\Phi} v_S U_{2i} + \lambda_\Phi v_\Phi U_{3i})U_{3j}U_{3k}. \quad (23)$$

The Yukawa couplings become

$$\mathcal{L}_{h_i f f} = - \sum_f \sum_{i=1}^3 \frac{m_f U_{1i}}{v} h_i \bar{f} f, \quad (24)$$

where f denotes the SM fermions.

The neutral current interactions arising from the $SU(2)_L \times U(1)_Y \times U(1)_X$ gauge symmetry are given by

$$\mathcal{L}_{\text{NC}} = B_\mu j_Y^\mu + W_\mu^3 j_3^\mu + X_\mu j_X^\mu, \quad (25)$$

with

$$j_Y^\mu = \sum_f g' (Y_{f,L} \bar{f}_L \gamma^\mu f_L + Y_{f,R} \bar{f}_R \gamma^\mu f_R), \quad (26)$$

$$j_3^\mu = \sum_f g T_f^3 \bar{f}_L \gamma^\mu f_L, \quad (27)$$

$$j_X^\mu = i g_X (S^\dagger \overleftrightarrow{\partial}^\mu S + 2\Phi^\dagger \overleftrightarrow{\partial}^\mu \Phi), \quad (28)$$

where T_f^3 is the third component of the weak isospin for a SM fermion f , and $Y_{f,L}$ and $Y_{f,R}$ are the weak hypercharges for left- and right-handed fermions. If we define $\hat{A}_\mu \equiv \hat{c}_W B_\mu + \hat{s}_W W_\mu^3$ and $\hat{Z}_\mu \equiv -\hat{s}_W B_\mu + \hat{c}_W W_\mu^3$, the neutral current interactions can be expressed in a familiar form

$$\mathcal{L}_{\text{NC}} = \hat{A}_\mu j_{\text{EM}}^\mu + \hat{Z}_\mu j_Z^\mu + X_\mu j_X^\mu, \quad (29)$$

with

$$j_{\text{EM}}^\mu = \sum_f Q_f e \bar{f} \gamma^\mu f, \quad (30)$$

$$\hat{j}_Z^\mu = \frac{g}{2\hat{c}_W} \sum_f \bar{f} \gamma^\mu (T_f^3 - 2Q_f \hat{s}_W^2 - T_f^3 \gamma^5) f, \quad (31)$$

where Q_f is the electric charge of f in units of $e = gg'/\sqrt{g^2 + g'^2}$.

The relation between $(\hat{A}_\mu, \hat{Z}_\mu, X_\mu)$ and the mass basis (A_μ, Z_μ, Z'_μ) is

$$\begin{pmatrix} \hat{A}_\mu \\ \hat{Z}_\mu \\ X_\mu \end{pmatrix} = R \begin{pmatrix} A_\mu \\ Z_\mu \\ Z'_\mu \end{pmatrix}, \quad (32)$$

where

$$R = \begin{pmatrix} \hat{c}_W & \hat{s}_W & 0 \\ -\hat{s}_W & \hat{c}_W & 0 \\ 0 & 0 & 1 \end{pmatrix} K = \begin{pmatrix} 1 & -\hat{c}_W t_\varepsilon s_\xi & -\hat{c}_W t_\varepsilon c_\xi \\ 0 & \hat{s}_W t_\varepsilon s_\xi + c_\xi & \hat{s}_W t_\varepsilon c_\xi - s_\xi \\ 0 & s_\xi/c_\varepsilon & c_\xi/c_\varepsilon \end{pmatrix}. \quad (33)$$

Therefore, the neutral current interactions in the mass basis are [37, 39]

$$\mathcal{L}_{\text{NC}} = A_\mu j_{\text{EM}}^\mu + Z_\mu j_Z^\mu + Z'_\mu j_{Z'}^\mu, \quad (34)$$

with

$$j_Z^\mu = \sum_f \bar{f} \gamma^\mu (g_{V,Z}^f - g_{A,Z}^f \gamma^5) f + \frac{s_\xi}{c_\varepsilon} j_X^\mu, \quad (35)$$

$$j_{Z'}^\mu = \sum_f \bar{f} \gamma^\mu (g_{V,Z'}^f - g_{A,Z'}^f \gamma^5) f + \frac{c_\xi}{c_\varepsilon} j_X^\mu, \quad (36)$$

where

$$g_{V,Z}^f = \frac{g}{2\hat{c}_W} (\hat{s}_W t_\varepsilon s_\xi + c_\xi) (T_f^3 - 2Q_f \hat{s}_W^2) - Q_f e \hat{c}_W t_\varepsilon s_\xi, \quad (37)$$

$$g_{A,Z}^f = \frac{g}{2\hat{c}_W} (\hat{s}_W t_\varepsilon s_\xi + c_\xi) T_f^3, \quad (38)$$

$$g_{V,Z'}^f = \frac{g}{2\hat{c}_W} (\hat{s}_W t_\varepsilon c_\xi - s_\xi) (T_f^3 - 2Q_f \hat{s}_W^2) - Q_f e \hat{c}_W t_\varepsilon c_\xi, \quad (39)$$

$$g_{A,Z'}^f = \frac{g}{2\hat{c}_W} (\hat{s}_W t_\varepsilon c_\xi - s_\xi) T_f^3. \quad (40)$$

Note that the electromagnetic current interactions $A_\mu j_{\text{EM}}^\mu$ remain in the SM form. For $\varepsilon = 0$, we have $A^\mu = \hat{A}^\mu$, $Z^\mu = \hat{Z}^\mu$, and $Z'^\mu = X^\mu$, and the Z couplings to the fermions are the same as in the SM, while the Z' boson only couples to j_X^μ . The existence of the kinetic mixing makes Z couple to j_X^μ and Z' couple to the SM fermions.

The Z - χ - h_i and Z' - χ - h_i couplings from the neutral current interactions $Z_\mu j_Z^\mu + Z'_\mu j_{Z'}^\mu$ are

$$\mathcal{L}_{\chi h_i} = \sum_{i=1}^3 (g_{Z\chi h_i} Z_\mu \chi \overleftrightarrow{\partial}^\mu h_i + g_{Z'\chi h_i} Z'_\mu \chi \overleftrightarrow{\partial}^\mu h_i), \quad (41)$$

where

$$g_{Z\chi h_i} = \frac{g_X s_\xi}{c_\varepsilon} (c_\beta U_{2i} - 2s_\beta U_{3i}), \quad (42)$$

$$g_{Z'\chi h_i} = \frac{g_X c_\xi}{c_\varepsilon} (c_\beta U_{2i} - 2s_\beta U_{3i}). \quad (43)$$

These couplings break the Z_2 symmetry $\chi \rightarrow -\chi$, inducing decay processes of the pNGB WIMP χ . In order to be a viable DM candidate, χ should have a sufficiently long lifetime.

The best measured electroweak quantities are the fine-structure constant $\alpha(m_Z)$ in the $\overline{\text{MS}}$ scheme, the Fermi constant G_F , and the Z boson pole mass m_Z . From these quantities, it is conventional to define the “physical” weak mixing parameters s_W^2 and $c_W^2 \equiv 1 - s_W^2$ via the tree-level SM relation [36, 40]

$$s_W^2 c_W^2 = \frac{\pi\alpha}{\sqrt{2}G_F m_Z^2}. \quad (44)$$

Then the hatted parameters \hat{s}_W^2 and \hat{c}_W^2 can be determined by [38]

$$s_W^2 c_W^2 (1 + \hat{s}_W t_\varepsilon t_\xi) = \hat{s}_W^2 \hat{c}_W^2. \quad (45)$$

The values of g and g' are settled by $g = e/\hat{s}_W$ and $g' = e/\hat{c}_W$ with $e = \sqrt{4\pi\alpha}$.

There are 10 free parameters in the model, which are chosen to be

$$v_S, v_\Phi, m_\chi, m_{h_2}, m_{h_3}, m_{Z'}, \lambda_{HS}, \lambda_{H\Phi}, \lambda_{S\Phi}, s_\varepsilon. \quad (46)$$

For a UV completion of the original pNGB DM model, we are particularly interested in the parameter regions with $v_\Phi \gg v_S \sim v$. This implies a mass hierarchy of $m_{Z'} \sim m_{h_3} \gg m_{h_2} \sim m_{h_1}$, leading to $r = m_{Z'}^2/m_Z^2 \gg 1$ and hence $|\xi| \ll |\varepsilon|$. Therefore, the value of \hat{s}_W would be very close to s_W for any value of s_ε .

The kinetic mixing contributes to the electroweak oblique parameters S , T , and U [41, 42] at tree level. For a small ε , we have

$$\xi \simeq \frac{s_W \varepsilon}{1 - r}, \quad (47)$$

and [43]

$$S \simeq \frac{4(c_W^2 - r)s_W^2 c_W^2 \varepsilon^2}{\alpha(1 - r)^2}, \quad T \simeq -\frac{r s_W^2 \varepsilon^2}{\alpha(1 - r)^2}, \quad U \simeq \frac{4s_W^4 c_W^2 \varepsilon^2}{\alpha(1 - r)^2}. \quad (48)$$

Because S , T , and U are all highly suppressed by r , we expect that the constraint on the oblique parameters from the global fit of electroweak precision measurements [44] would not constrain our interested parameter regions.

III. PHENOMENOLOGY

In this section, we discuss the phenomenological consequences of the model.

A. WIMP-nucleon Scattering

In the original pNGB DM model with a directly introduced soft breaking parameter $\mu_S'^2$, the WIMP-nucleon scattering amplitude exactly vanishes at tree level in the zero momentum transfer limit [6]. Our UV completion gives $\mu_S'^2$ a dynamical origin, but inevitably introduces the χ - χ - ϕ coupling, leading to a nonvanishing χ -nucleon scattering amplitude. Nonetheless, we expect that the amplitude is significantly suppressed by a high UV scale v_Φ , since the $v_\Phi \rightarrow \infty$ limit recovers the original model.

The spin-independent (SI) χ -nucleon scattering is induced by the χ -quark scattering via t -channel exchanges of the CP -even Higgs bosons h_1 , h_2 , and h_3 . In the zero momentum transfer limit, the tree-level χ -quark scattering amplitude becomes

$$\begin{aligned} i\mathcal{M} &= \frac{im_q}{v} \bar{u}(k_2)u(k_1) \left(\frac{g_{h_1\chi^2}U_{11}}{m_{h_1}^2} + \frac{g_{h_2\chi^2}U_{12}}{m_{h_2}^2} + \frac{g_{h_3\chi^2}U_{13}}{m_{h_3}^2} \right), \\ &= \frac{im_q}{v} \bar{u}(k_2)u(k_1) \begin{pmatrix} g_{h_1\chi^2} & g_{h_2\chi^2} & g_{h_3\chi^2} \end{pmatrix} \begin{pmatrix} m_{h_1}^{-2} & & \\ & m_{h_2}^{-2} & \\ & & m_{h_3}^{-2} \end{pmatrix} U^T \begin{pmatrix} 1 \\ 0 \\ 0 \end{pmatrix}, \end{aligned} \quad (49)$$

where $u(k_1)$ and $\bar{u}(k_2)$ denote the plane-wave spinor coefficients for the incoming and outgoing quarks q of 4-momenta k_1 and k_2 . It is equivalent [6, 14] to express the amplitude in the interaction basis (h, s, ϕ) , whose couplings to χ are given by $G = (g_{h\chi^2} \ g_{s\chi^2} \ g_{\phi\chi^2})$ with

$$g_{h\chi^2} = (\lambda_{HS}c_\beta^2 + \lambda_{H\Phi}s_\beta^2)v, \quad (50)$$

$$g_{s\chi^2} = \lambda_S v_S c_\beta^2 + \lambda_{S\Phi} v_S s_\beta^2 + 2\mu_{S\Phi} s_\beta c_\beta, \quad (51)$$

$$g_{\phi\chi^2} = \lambda_\Phi v_\Phi s_\beta^2 + (\lambda_{S\Phi} v_\Phi + \mu_{S\Phi})c_\beta^2. \quad (52)$$

Utilizing $\text{diag}(m_{h_1}^{-2}, m_{h_2}^{-2}, m_{h_3}^{-2}) = U^T (M_E^2)^{-1} U$ and $(g_{h_1\chi^2} \ g_{h_2\chi^2} \ g_{h_3\chi^2}) = GU$, we derive

$$i\mathcal{M} = \frac{im_q}{v} \bar{u}(k_2)u(k_1) G (M_E^2)^{-1} \begin{pmatrix} 1 \\ 0 \\ 0 \end{pmatrix}. \quad (53)$$

Expanding the scattering amplitude in orders of v_Φ for $v_\Phi \gg v, v_S$, we obtain

$$i\mathcal{M} \simeq \frac{i\tilde{\lambda}m_q m_\chi^2}{2v^2 v_\Phi^2} \bar{u}(k_2)u(k_1) + \mathcal{O}(v_\Phi^{-4}), \quad (54)$$

where

$$\tilde{\lambda} = \frac{\lambda_{H\Phi}\lambda_{S\Phi} - \lambda_\Phi\lambda_{HS} + 2\lambda_{HS}\lambda_{S\Phi} - 2\lambda_S\lambda_{H\Phi}}{\lambda_H\lambda_S\lambda_\Phi + 2\lambda_{HS}\lambda_{H\Phi}\lambda_{S\Phi} - \lambda_S\lambda_{H\Phi}^2 - \lambda_\Phi\lambda_{HS}^2 - \lambda_H\lambda_{S\Phi}^2}. \quad (55)$$

Thus, the amplitude is suppressed by v_Φ^{-2} , as expected. Based on effective field theory [45], we

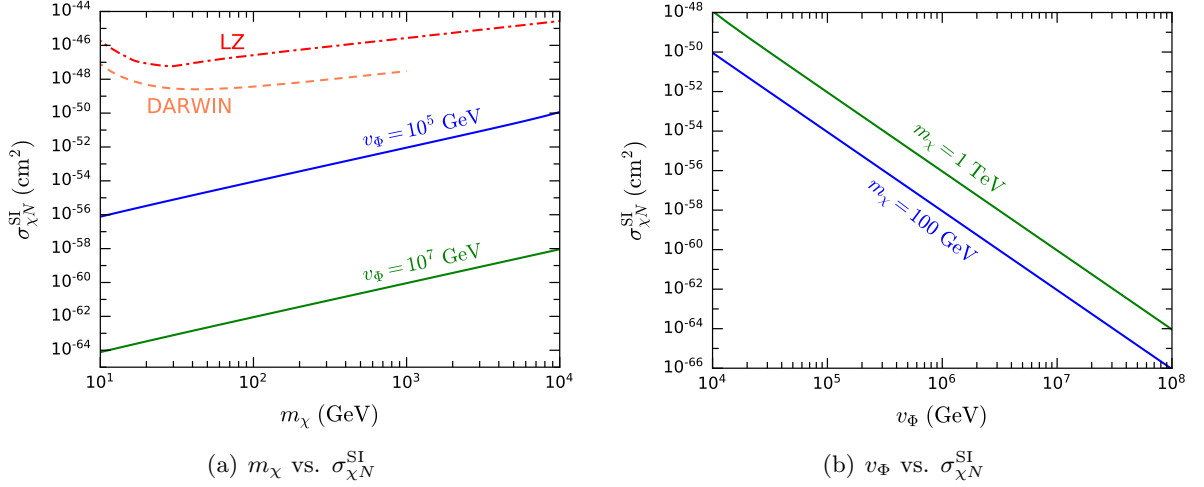


FIG. 1. SI χ -nucleon scattering cross section $\sigma_{\chi N}^{\text{SI}}$ as functions of m_χ (a) and v_Φ (b). The blue and green lines in the left (right) panel correspond to $v_\Phi = 10^5$ GeV ($m_\chi = 100$ GeV) and $v_\Phi = 10^7$ GeV ($m_\chi = 1$ TeV), respectively. Other parameters are fixed as $v_S = 1$ TeV, $m_{h_2} = 300$ GeV, $m_{h_3} = 0.1v_\Phi$, $\lambda_{HS} = 0.03$, and $\lambda_{H\Phi} = \lambda_{S\Phi} = 0.01$. The left panel also shows the 90% C.L. constraint from the LZ direct detection experiment [5] as well as the future sensitivity of the DARWIN experiment [47].

derive the resulting SI χ -nucleon scattering cross section

$$\sigma_{\chi N}^{\text{SI}} \simeq \frac{\tilde{\lambda}^2 m_N^4 m_\chi^4 [2 + 7(f_u^N + f_d^N + f_s^N)]^2}{1296\pi(m_N + m_\chi)^2 v^4 v_\Phi^4} + \mathcal{O}(v_\Phi^{-6}), \quad (56)$$

which is suppressed by v_Φ^{-4} . Here, $f_{u,d,s}^N$ are the nucleon form factors for light quarks [46].

In Fig. 1(a), we plot the χ -nucleon scattering cross section $\sigma_{\chi N}^{\text{SI}}$ as functions of m_χ for $v_\Phi = 10^5$ and 10^7 GeV, with the other related parameters fixed to be $v_S = 1$ TeV, $m_{h_2} = 300$ GeV, $m_{h_3} = 0.1v_\Phi$, $\lambda_{HS} = 0.03$, and $\lambda_{H\Phi} = \lambda_{S\Phi} = 0.01$. For $m_\chi \gg m_N$, Eq. (56) shows that $\sigma_{\chi N}^{\text{SI}}$ is proportional to m_χ^2 . Therefore, as m_χ increases by one order of magnitudes, $\sigma_{\chi N}^{\text{SI}}$ in Fig. 1(a) increases by two orders of magnitudes. $v_\Phi = 10^7$ GeV leads to cross sections smaller than those for $v_\Phi = 10^5$ GeV by eight orders of magnitudes, because of $\sigma_{\chi N}^{\text{SI}} \propto v_\Phi^{-4}$. Note that $v_\Phi = 10^5$ GeV results in $\sigma_{\chi N}^{\text{SI}}$ much smaller than the 90% confidence level (C.L.) upper limits from the recent LZ direct detection experiment [5], and even beyond the reach of the future DARWIN experiment with a 200 t · yr exposure [47]. Fig. 1(b) displays $\sigma_{\chi N}^{\text{SI}}$ as functions of v_Φ for $m_\chi = 100$ GeV and 1 TeV, demonstrating an obvious $\sigma_{\chi N}^{\text{SI}} \propto v_\Phi^{-4}$ behavior.

B. WIMP Lifetime

The Z - χ - h_i and Z' - χ - h_i couplings (41) induce the decay of the pNGB WIMP χ . We are particularly interested in the parameter regions with $m_\chi \ll m_{Z'} \sim m_{h_3}$, where the χ decay processes involve $\chi \rightarrow h_i^{(*)} Z^{(*)}$ and $\chi \rightarrow h_i^{(*)} Z'^*$. Depending on the mass spectrum, the h_1 , h_2 , and Z bosons could be either on or off shell, while the h_3 and Z' bosons must be off shell. The corresponding Feynman diagrams are depicted in Fig. 2.

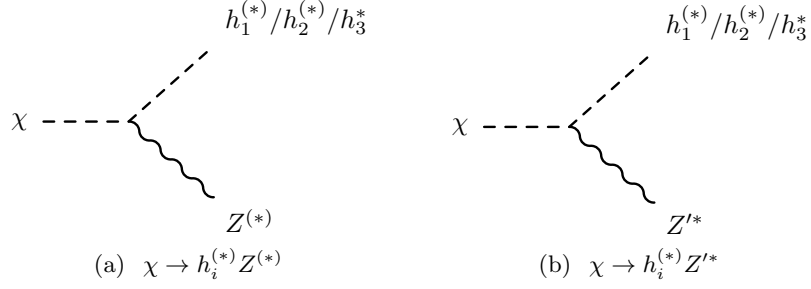


FIG. 2. Feynman diagrams for χ decays into $h_i^{(*)} Z^{(*)}$ (a) and $h_i^{(*)} Z'^{*}$ (b), where h_1 , h_2 , and Z could be either on or off shell, while h_3 and Z' must be off shell for $m_\chi \ll m_{h_3}, m_{Z'}$.

Six years of Fermi-LAT γ -ray observations of dwarf galaxies imply a conservative constraint on the WIMP lifetime, $\tau_\chi \gtrsim 10^{27}$ s [48], corresponding to a bound on the total WIMP decay width, $\Gamma_\chi \equiv 1/\tau_\chi \lesssim 6.6 \times 10^{-52}$ GeV. In the $v_\Phi \rightarrow \infty$ limit, all the χ decay channels are forbidden, and χ becomes stable. Thus, the constraint on the χ lifetime is expected to give a lower bound on the UV scale v_Φ . Therefore, the total decay width of the pNGB WIMP χ should be carefully calculated.

When $m_\chi > m_{h_i} + m_Z$ ($i = 1, 2$), the 2-body partial decay width of $\chi \rightarrow h_i Z$ is given by

$$\Gamma(\chi \rightarrow h_i Z) = \frac{g_{Z\chi h_i}^2 m_\chi^3}{16\pi m_Z^2} \lambda^{3/2} \left(1, \frac{m_{h_i}^2}{m_\chi^2}, \frac{m_Z^2}{m_\chi^2} \right), \quad (57)$$

where the λ function is defined as $\lambda(x, y, z) = x^2 + y^2 + z^2 - 2xy - 2xz - 2yz$. When $m_\chi > m_{h_i} + 2m_f$ ($i = 1, 2$), we should consider the 3-body decays $\chi \rightarrow h_i f \bar{f}$. If $m_{h_i} + 2m_f < m_\chi < m_{h_i} + m_Z$, both the Feynman diagrams mediated by the off-shell Z and Z' bosons contribute to $\chi \rightarrow h_i f \bar{f}$. However, once the 2-body decay channels $\chi \rightarrow h_i Z$ open, the $\chi \rightarrow h_i f \bar{f}$ decay diagrams mediated by the Z bosons should be discarded for avoiding double counting. When $m_Z + 2m_f < m_\chi < m_{h_i} + m_Z$ ($i = 1, 2$), the 3-body decays $\chi \rightarrow Z f \bar{f}$ mediated by h_i should be involved. Since the fermion couplings to h_i are commonly suppressed by m_f/v , the dominant contributions to $\chi \rightarrow Z f \bar{f}$ come from the heaviest SM fermions t , b , τ , and c . If $2m_W + m_Z < m_\chi < m_{h_2} + m_Z$, the 3-body decays $\chi \rightarrow W^+ W^- Z$ and $\chi \rightarrow Z Z Z$ mediated by off-shell h_i bosons may happen. Nonetheless, our calculation shows that their contributions are negligible, compared to $\chi \rightarrow Z f \bar{f}$ and $\chi \rightarrow h_i f \bar{f}$. If all 2- and 3-body decay channels are kinematically forbidden, the 4-body decays $\chi \rightarrow f \bar{f} f' \bar{f}'$ should be taken into account.

For calculating the 3-body partial decay widths, we derive analytic expressions and perform numerical integrals. Since the Feynman diagrams and integrals for the 4-body decays are too complicated to be dealt with by hand, we utilize the Monte Carlo tool **MadGraph5_aMG@NLO** [49] to automatically evaluate the 4-body partial decay widths. In the latter approach, **FeynRules** [50] is used to implement the model.

We fix the parameters as $v_S = 1$ TeV, $m_{h_2} = 300$ GeV, $m_{h_2} = m_{Z'} = 0.1v_\Phi$, $\lambda_{HS} = 0.03$, $\lambda_{H\Phi} = \lambda_{S\Phi} = 0.01$, and $\sin \varepsilon = 0.1$, and show the total decay width of χ as functions of m_χ for $v_\Phi = 10^{10}$, 10^{13} , and 10^{15} GeV in Fig. 3(a). The threshold effects at $m_\chi = m_{h_1} \simeq 125$ GeV,

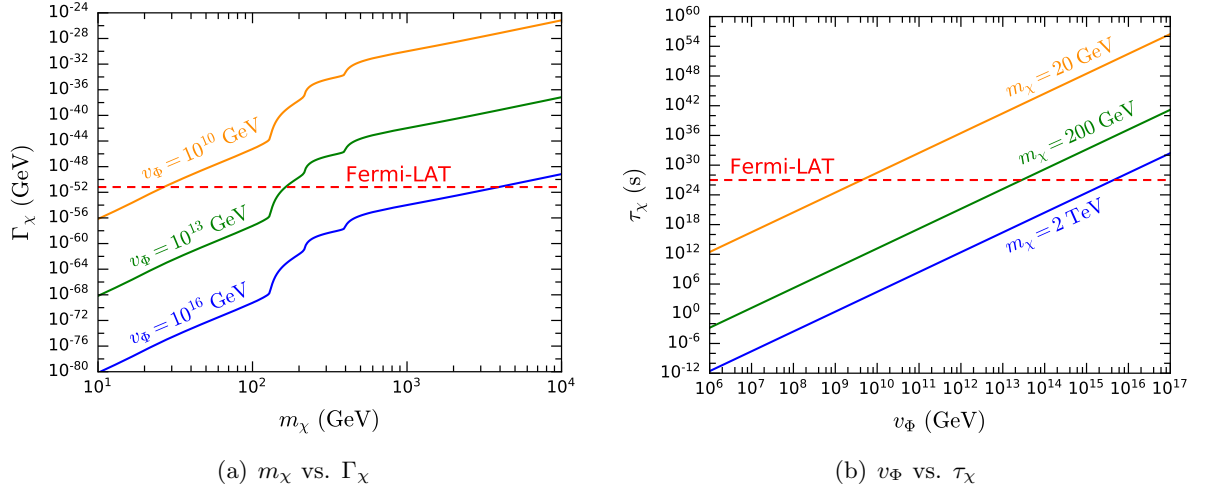


FIG. 3. χ decay width Γ_χ as functions of m_χ for $v_\Phi = 10^{10}$, 10^{13} , and 10^{15} GeV (a) and χ lifetime τ_χ as functions of v_Φ for $m_\chi = 20$, 200, and 2000 GeV (b). Other parameters are fixed as $v_S = 1$ TeV, $m_{h_2} = 300$ GeV, $m_{h_3} = m_{Z'} = 0.1v_\Phi$, $\lambda_{HS} = 0.03$, $\lambda_{H\Phi} = \lambda_{S\Phi} = 0.01$, and $\sin \varepsilon = 0.1$. The dashed lines denote the conservative constraint $\tau_\chi \gtrsim 10^{27}$ s from Fermi-LAT γ -ray observations of dwarf galaxies [48].

$m_\chi = m_{h_1} + m_Z \simeq 216$ GeV, and $m_\chi = m_{h_2} + m_Z \simeq 391$ GeV are clearly demonstrated. The red dashed line denotes the Fermi-LAT bound on the WIMP lifetime [48] converted to the total decay width, $\Gamma_\chi \lesssim 6.6 \times 10^{-52}$ GeV. Thus, $m_\chi \gtrsim 25$, 140, and 3900 GeV are excluded for $v_\Phi = 10^{10}$, 10^{13} , and 10^{15} GeV, respectively. In Fig. 3(b), we display the χ lifetime as functions of v_Φ for $m_\chi = 20$, 200, and 2000 GeV, where the Fermi-LAT constraint excludes $v_\Phi \lesssim 4 \times 10^9$, 3×10^{13} , and 4×10^{15} GeV, respectively. Thus, the bound on v_Φ given by the WIMP lifetime is much more stringent than the bound from direct detection experiments.

C. Higgs Physics

In this model, the properties of the SM-like Higgs boson h_1 deviate from the SM prediction. The tree-level h_1 couplings to SM particles can be parametrized as

$$\mathcal{L}_{h_1} = \kappa_W \frac{2m_W^2}{v} h_1 W_\mu^+ W^{-,\mu} + \kappa_Z \frac{m_Z^2}{v} h_1 Z_\mu Z^\mu - \sum_f \kappa_f \frac{m_f}{v} h_1 \bar{f} f, \quad (58)$$

where κ_W , κ_Z , and κ_f are the modifiers to the couplings with W , Z , and fermions. The SM corresponds to $\kappa_W = \kappa_Z = \kappa_f = 1$, while this model gives

$$\kappa_W = \kappa_f = U_{11}, \quad (59)$$

$$\kappa_Z = U_{11} c_\xi^2 (1 + \hat{s}_W t_\varepsilon t_\xi) + \frac{s_\xi^2 g_X^2 v}{c_\varepsilon^2 m_Z^2} (U_{21} v_S + 4U_{31} v_\Phi). \quad (60)$$

In addition, exotic Higgs decay channels may exist. If $m_{h_1} > 2m_\chi$, the invisible decay channel

$h_1 \rightarrow \chi\chi$ opens, leading to an invisible decay width

$$\Gamma(h_1 \rightarrow \chi\chi) = \frac{g_{h_1\chi\chi}^2}{32\pi m_{h_1}} \sqrt{1 - \frac{4m_\chi^2}{m_{h_1}^2}}. \quad (61)$$

If $m_{h_1} > m_\chi + m_Z$, there is a semi-invisible decay channel $h_1 \rightarrow \chi Z$ with a partial decay width

$$\Gamma(h_1 \rightarrow \chi Z) = \frac{g_{Z\chi h_1}^2 m_{h_1}^3}{16\pi m_Z^2} \lambda^{3/2} \left(1, \frac{m_\chi^2}{m_{h_1}^2}, \frac{m_Z^2}{m_{h_1}^2} \right), \quad (62)$$

If $m_{h_1} > 2m_{h_2}$, the partial decay width of $h_1 \rightarrow h_2 h_2$ is given by

$$\Gamma(h_1 \rightarrow h_2 h_2) = \frac{(g_{h_1 h_2 h_2} + g_{h_2 h_1 h_2} + g_{h_2 h_2 h_1})^2}{8\pi m_{h_1}} \sqrt{1 - \frac{4m_{h_2}^2}{m_{h_1}^2}}. \quad (63)$$

We utilize a numerical tool `Lilith 2` [51, 52] to constrain the model parameter space with the LHC Higgs measurements based on the `Lilith` database of version 19.09, including ATLAS and CMS Run 2 data of integrated luminosity 36 fb^{-1} . The important results sensitive to this model come from the measurements of $h_1 \rightarrow \gamma\gamma$ [53], $h_1 \rightarrow ZZ$ [54], and $h_1 \rightarrow W^+W^-$ [55], and the search for invisible Higgs decays [56], and the combined measurements of the Higgs couplings from several channels [57]. For each parameter point, `Lilith` constructs an approximate likelihood function from the measurements of the Higgs signal strengths. The corresponding p -value larger than 0.05 is required, ensuring that each viable parameter point is consistent with the experimental results at 95% C.L.

D. WIMP Annihilation

The relic abundance of the pNGB WIMP χ is essentially determined by $\chi\chi$ annihilation cross section at the freeze-out epoch, $\langle\sigma_{\text{ann}}v\rangle_{\text{FO}}$. Potential $\chi\chi$ annihilation channels include $f\bar{f}$, W^+W^- , ZZ , and $h_i h_j$ ($i, j = 1, 2$). The related Feynman diagrams are enormous. We make use of a `MadGraph5_aMG@NLO` plugin `MadDM` [58] to automatically generate and calculate all tree-level annihilation diagrams, and to solve the Boltzmann equation for predicting the relic abundance $\Omega_\chi h^2$.

$\chi\chi$ annihilation would still occur at the present day, inducing potential γ -ray signals in indirect detection experiments. A combined search for such γ -ray signals in the dwarf galaxies from the Fermi-LAT space experiment and the MAGIC Cherenkov telescopes [59] have given important constraints on the DM annihilation cross section. We further utilize `MadGraph5_aMG@NLO` [49] to evaluate the $\chi\chi$ annihilation cross section at a typical average WIMP velocity 2×10^{-5} for dwarf galaxies, $\langle\sigma_{\text{ann}}v\rangle_{\text{D}}$. Thus, the Fermi-MAGIC result can be used to constrain the model.

IV. PARAMETER SCAN

We perform a random scan in the following parameter ranges,

$$\begin{aligned} 10 \text{ GeV} < v_S, m_{h_2}, m_\chi < 10^4 \text{ GeV}, \quad 10^9 \text{ GeV} < v_\Phi < 10^{17} \text{ GeV}, \\ 10^8 \text{ GeV} < m_{h_3}, m_{Z'} < 10^{16} \text{ GeV}, \quad 0.01 < |s_\varepsilon| < 0.9, \\ 10^{-3} < |\lambda_{HS}|, |\lambda_{H\Phi}|, |\lambda_{S\Phi}| < 1. \end{aligned} \quad (64)$$

The induced couplings λ_H , λ_S , λ_Φ , and g_X are further required to range from 10^{-3} to 1. We select the parameter points that satisfy the phenomenological requirements below.

- The WIMP lifetime satisfies the Fermi-LAT bound $\tau_\chi \gtrsim 10^{27} \text{ s}$ [48].
- The signal strengths of the 125 GeV Higgs boson h_1 are consistent with the Higgs measurements after LHC Run 2 at 95% C.L. according to the `Lilith` calculation.
- The predicted WIMP relic abundance $\Omega_\chi h^2$ lies within the 3σ range of the Planck measurement $\Omega_{\text{DM}} h^2 = 0.1200 \pm 0.0012$ [60].

We project the selected parameter points onto the v_S - m_{h_2} , v_Φ - m_{h_3} , v_Φ - $m_{Z'}$, and $m_{Z'}$ - $|\xi|$ planes in Figs. 4(a), 4(b), 4(c), and 4(d), with color axes corresponding to λ_S , λ_Φ , g_X , and $|s_\varepsilon|$, respectively. Since we focus on the parameter region with $v_\Phi \gg v, v_S, m_\chi$, the mass-squared matrix (6) implies $m_{h_3}^2 \simeq \lambda_\Phi v_\Phi^2$, which is clearly shown in Fig. 4(b). More precisely, this plot demonstrates that m_{h_3} is proportional to v_Φ and positively correlated to λ_Φ . For $|\lambda_{HS}| \ll 1$, Eq. (6) leads to $m_{h_2}^2 \simeq \lambda_S v_S^2$. Nonetheless, such positive correlations of m_{h_2} to v_S and λ_S do not totally manifest in Fig. 4(a). The exceptions should be due to large $|\lambda_{HS}|$.

According to Eqs. (18) and (20), $v_\Phi, m_{Z'} \gg v, v_S$ means that $m_{Z'} \simeq 2g_X v_\Phi / c_\varepsilon$ and $t_\xi \simeq -s_W t_\varepsilon m_Z^2 / m_{Z'}^2$. Fig. 4(c) illustrates the positive correlations of $m_{Z'}$ to v_Φ and g_X , while Fig. 4(d) displays the negative (positive) correlation of $|\xi|$ to $m_{Z'}$ ($|s_\varepsilon|$). From Figs. 4(b) and 4(c), we find that the lower limit of the UV scale v_Φ is down to $\sim 10^{10} \text{ GeV}$, given by the Fermi-LAT constraint on the WIMP lifetime.

In Fig. 5(a), we demonstrate the selected parameter points in the Γ_{h_1} -($1 - \kappa_Z$) plane, with colors denoting $1 - U_{11}$. For $v_\Phi, m_{Z'} \gg v, v_S$, Eq. (60) becomes $\kappa_Z \simeq U_{11} = \kappa_W = \kappa_f$, and thus the color axis is basically identical to the vertical axis in Fig. 5(a). There is an obvious curve constituted by parameter points in this plot, indicating the positive correlation between the h_1 total decay width Γ_{h_1} and κ_Z (or U_{11} , equivalently). The exceptional parameter points have larger Γ_{h_1} , which are contributed by the exotic Higgs decays $h_1 \rightarrow \chi\chi$, $h_1 \rightarrow \chi Z$, and $h_1 \rightarrow h_2 h_2$. We can see that the constraints from current LHC Higgs measurements give $1 - \kappa_Z \lesssim 0.1$ (or $U_{11} \gtrsim 0.9$) and $3.3 \text{ MeV} \lesssim \Gamma_{h_1} \lesssim 5 \text{ MeV}$.

Future experiments at the planning Higgs factories, such as CEPC [61], FCC-ee [62], and ILC [63], would be rather sensitive to κ_Z , κ_W , κ_b , and Γ_{h_1} . For instance, the 1σ precision of the CEPC measurements on these quantities are estimated to be $\delta\kappa_Z = 0.25\%$, $\delta\kappa_W = 1.4\%$, $\delta\kappa_b = 1.3\%$, and $\delta\Gamma_{h_1} = 2.8\%$ [61]. Figure 5(a) also shows the expected 95% C.L. coverage

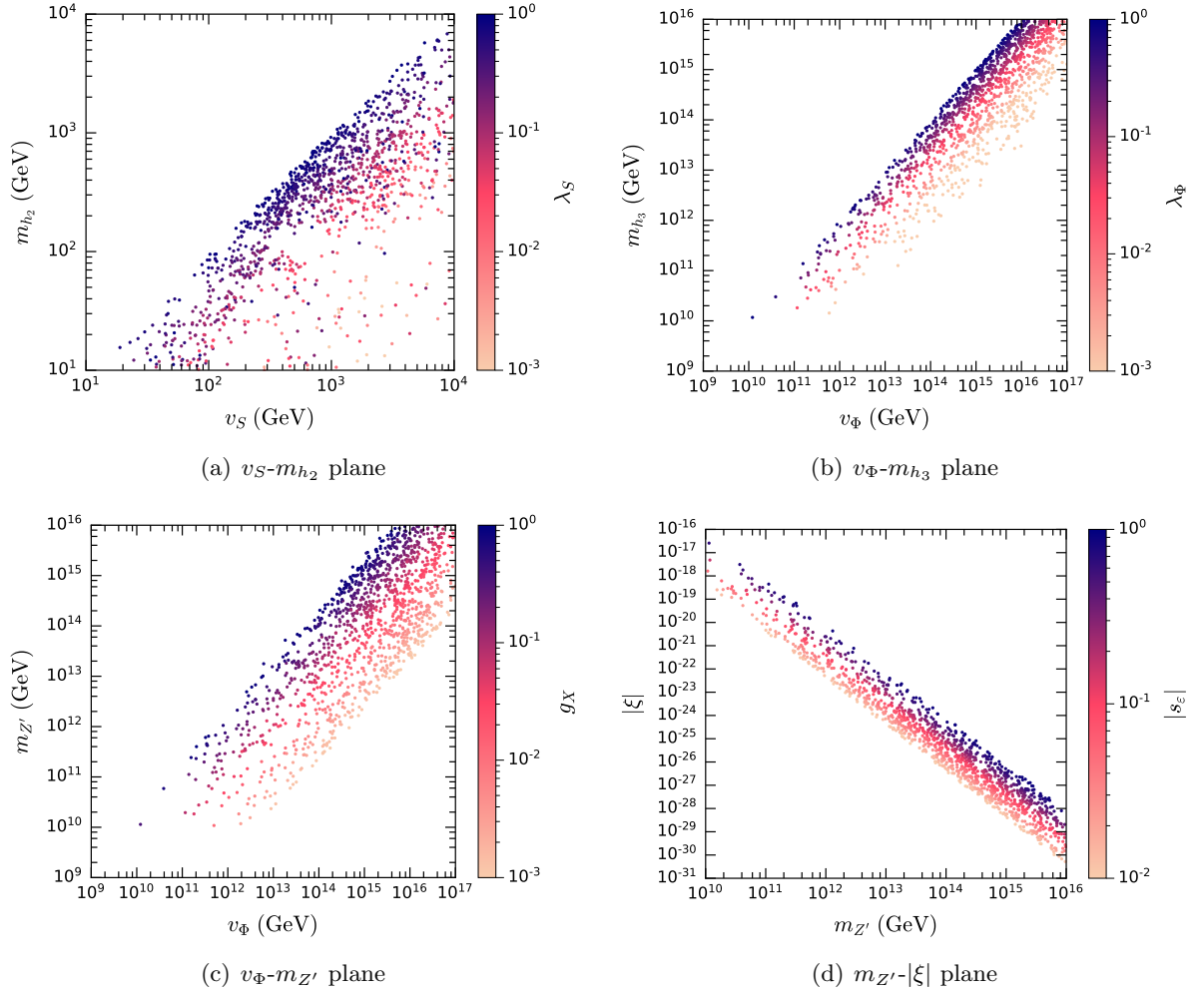


FIG. 4. Selected parameter points projected onto the v_S - m_{h_2} (a), v_Φ - m_{h_3} (b), v_Φ - $m_{Z'}$ (c), and $m_{Z'}$ - $|\xi|$ (d) planes, with color axes corresponding to λ_S , λ_Φ , g_X , and $|s_\varepsilon|$, respectively.

of the CEPC experiment on κ_Z and Γ_{h_1} , and a large fraction of the selected parameter points would be properly tested.

Moreover, the CEPC project could also constrain the invisible Higgs decay branching ratio BR_{inv} down to 0.3% at 95% C.L. [61]. In this model, we have nonzero $\text{BR}_{\text{inv}} = \Gamma(h_1 \rightarrow \chi\chi)/\Gamma_{h_1}$ for $m_\chi < m_{h_1}/2$. Figure 5(b) displays the selected parameter points projected onto the m_χ - BR_{inv} plane. Current LHC data allow the parameter points with $\text{BR}_{\text{inv}} \lesssim 14\%$, while the CEPC experiment could probe most of the parameter points with $m_\chi < m_{h_1}/2$.

In Fig. 6(a), the selected parameter points are presented in the $\Omega_\chi h^2$ - $\langle\sigma_{\text{ann}}v\rangle_{\text{FO}}$ plane, with a color axis indicating the pNGB WIMP mass m_χ and colored regions corresponding to the 1σ , 2σ , and 3σ ranges of the relic abundance $\Omega_{\text{DM}} h^2 = 0.1200 \pm 0.0012$ measured by the Planck experiment [60]. The majority of the parameter points gather around the standard annihilation cross section $\langle\sigma_{\text{ann}}v\rangle_{\text{FO}} \sim 2 \times 10^{-26} \text{ cm}^3/\text{s}$. The rest points with nonstandard freeze-out annihilation cross sections should arise from resonance or threshold effects of specific annihilation channels that leads to velocity-dependent cross sections [64].

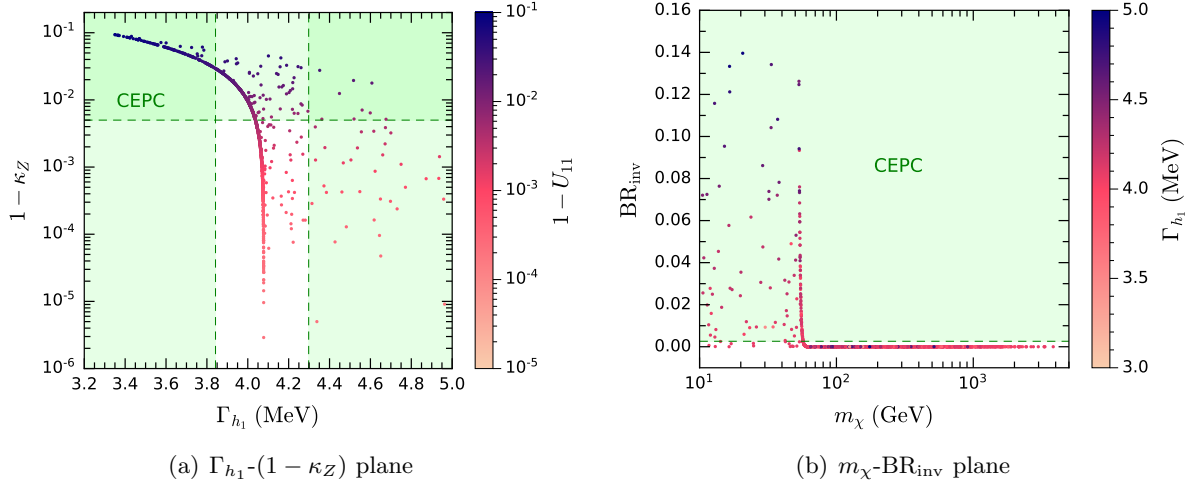


FIG. 5. Selected parameter points projected onto the Γ_{h_1} -($1 - \kappa_Z$) (a) and m_χ -BR_{inv} (b) planes, with color axes corresponding to $1 - U_{11}$ and Γ_{h_1} , respectively. The green regions denote the expected coverage of the future CEPC experiment at 95% C.L. [61].

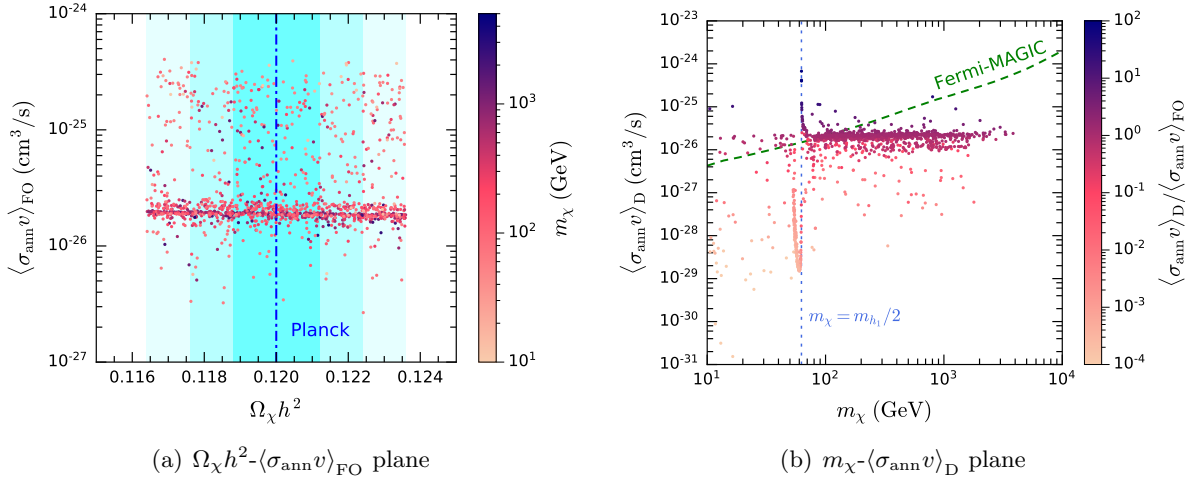


FIG. 6. Selected parameter points projected onto the $\Omega_\chi h^2$ - $\langle\sigma_{\text{ann}}v\rangle_{\text{FO}}$ (a) and m_χ - $\langle\sigma_{\text{ann}}v\rangle_{\text{D}}$ (b) planes, with color axes corresponding to m_χ and $\langle\sigma_{\text{ann}}v\rangle_{\text{D}} / \langle\sigma_{\text{ann}}v\rangle_{\text{FO}}$, respectively. The blue dot-dashed line and the colored regions in the left panel indicate the central value and the 1σ , 2σ , and 3σ ranges of the Planck measured relic abundance $\Omega_{\text{DM}} h^2 = 0.1200 \pm 0.0012$ [60]. In the right panel, the green dashed line denotes the upper limits from the Fermi-MAGIC γ -ray observations of dwarf galaxies at 95% C.L. [59], while the blue dotted line corresponds to $m_\chi = m_{h_1}/2$.

The selected parameter points are further shown in the m_χ - $\langle\sigma_{\text{ann}}v\rangle_{\text{D}}$ plane in Fig. 6(b), where the color axis denotes the ratio of $\langle\sigma_{\text{ann}}v\rangle_{\text{D}}$ to $\langle\sigma_{\text{ann}}v\rangle_{\text{FO}}$. $\langle\sigma_{\text{ann}}v\rangle_{\text{D}} \simeq \langle\sigma_{\text{ann}}v\rangle_{\text{FO}}$ means that $\chi\chi$ annihilation is s -wave dominated, corresponding to the standard case. The velocity dependence induced by the resonance or threshold effects would make $\langle\sigma_{\text{ann}}v\rangle_{\text{D}}$ different from $\langle\sigma_{\text{ann}}v\rangle_{\text{FO}}$. It is obvious that the parameter points with $\langle\sigma_{\text{ann}}v\rangle_{\text{D}} \neq \langle\sigma_{\text{ann}}v\rangle_{\text{FO}}$ around the $m_\chi = m_{h_1}/2$ line in Fig. 6(b) are caused by the h_1 resonance effect, while the h_2 resonance effect leads to $\langle\sigma_{\text{ann}}v\rangle_{\text{D}} \neq \langle\sigma_{\text{ann}}v\rangle_{\text{FO}}$ for some of the rest parameter points. The green dashed line in

Fig. 6(b) indicates the 95% C.L. upper limits of $\langle\sigma_{\text{ann}}v\rangle_{\text{D}}$ from the Fermi-MAGIC observations of dwarf galaxies assuming a $b\bar{b}$ annihilation channel. These limits can be approximately used to constrain the model. We find that only a small fraction of the selected parameter points have been excluded.

V. CONCLUSIONS AND DISCUSSIONS

In this paper, we have constructed a UV-complete model for pNGB dark matter with a hidden $U(1)_X$ gauge symmetry. Two complex scalar fields S and Φ carrying $U(1)_X$ charges of 1 unit and 2 units are introduced. The development of the Φ VEV v_Φ at a high scale breaks the $U(1)_X$ gauge symmetry into an approximate $U(1)_X$ global symmetry, which is softly broken by the $\mu_{S\Phi}$ term, leading to the desired pNGB WIMP DM setup. As a result, the tree-level WIMP-nucleon scattering is suppressed by the UV scale v_Φ . We have found a scaling relation $\sigma_{\chi N}^{\text{SI}} \propto v_\Phi^{-4}$, and hence $v_\Phi \gtrsim 10^5$ is high enough to escape direct detection.

Compared to the UV-completion with the $U(1)_{B-L}$ gauge symmetry [17, 18], our model does not need to introduce right-handed neutrinos for anomaly cancellation. Moreover, since the SM fermions do not carry $U(1)_X$ charges, the interactions leading to WIMP decays are reduced. Specifically, the interactions that induce WIMP decays only originate from the kinetic mixing between the $U(1)_X$ and $U(1)_Y$ gauge fields. This would relatively relieve the WIMP lifetime constraint on the UV scale v_Φ .

A random scan in the parameter space has been carried out to obtain the parameter points satisfying the phenomenological constraints from the WIMP lifetime, the 125 GeV Higgs measurements, the observed DM relic abundance, and indirect detection of WIMP annihilation. We have found that the WIMP lifetime bound from the Fermi-LAT γ -ray observations has set a lower limit on the UV scale, $v_\Phi \gtrsim 10^{10}$ GeV, which is indeed looser than $v_\Phi \gtrsim \mathcal{O}(10^{11}-10^{13})$ GeV in the $U(1)_{B-L}$ case estimated in Refs. [17, 18]. The parameter points satisfying current LHC Higgs measurements have $U_{11} \gtrsim 0.9$, $3.3 \text{ MeV} \lesssim \Gamma_{h_1} \lesssim 5 \text{ MeV}$, and $\text{BR}_{\text{inv}} \lesssim 14\%$. A large fraction of these parameter points could be properly tested by future Higgs factories.

Additional constraints on this model come from direct searches for the h_2 boson at the 13 TeV LHC from decay channels such as $h_2 \rightarrow ZZ$ [65, 66], $h_2 \rightarrow W^+W^-$ [67, 68], $h_2 \rightarrow t\bar{t}$ [69], and $h_2 \rightarrow h_1h_1$ [70]. By reinterpreting these constraints, some parameter points remaining in our scan may have been excluded. Nonetheless, the h_2 couplings to the W and Z bosons and to the top quark are highly suppressed by the mixing parameter U_{12} . Thus, we expect most of the parameter points are still available.

ACKNOWLEDGMENTS

This work is supported in part by the National Natural Science Foundation of China under Grants No. 11875327, No. 11905300, and No. 11805288, the Fundamental Research Funds for

the Central Universities, and the Sun Yat-Sen University Science Foundation.

-
- [1] G. Bertone, D. Hooper, and J. Silk, “Particle dark matter: Evidence, candidates and constraints,” *Phys. Rept.* **405** (2005) 279–390, [arXiv:hep-ph/0404175 \[hep-ph\]](#).
 - [2] J. L. Feng, “Dark Matter Candidates from Particle Physics and Methods of Detection,” *Ann. Rev. Astron. Astrophys.* **48** (2010) 495–545, [arXiv:1003.0904 \[astro-ph.CO\]](#).
 - [3] B.-L. Young, “A survey of dark matter and related topics in cosmology,” *Front. Phys.(Beijing)* **12** (2017) 121201. [Erratum: *Front. Phys.(Beijing)*12,no.2,121202(2017)].
 - [4] **PandaX-4T** Collaboration, Y. Meng *et al.*, “Dark Matter Search Results from the PandaX-4T Commissioning Run,” *Phys. Rev. Lett.* **127** (2021) 261802, [arXiv:2107.13438 \[hep-ex\]](#).
 - [5] J. Aalbers *et al.*, “First Dark Matter Search Results from the LUX-ZEPLIN (LZ) Experiment,” [arXiv:2207.03764 \[hep-ex\]](#).
 - [6] C. Gross, O. Lebedev, and T. Toma, “Cancellation Mechanism for Dark-Matter–Nucleon Interaction,” *Phys. Rev. Lett.* **119** (2017) 191801, [arXiv:1708.02253 \[hep-ph\]](#).
 - [7] D. Azevedo, M. Duch, B. Grzadkowski, D. Huang, M. Iglicki, and R. Santos, “One-loop contribution to dark-matter-nucleon scattering in the pseudo-scalar dark matter model,” *JHEP* **01** (2019) 138, [arXiv:1810.06105 \[hep-ph\]](#).
 - [8] K. Ishiwata and T. Toma, “Probing pseudo Nambu-Goldstone boson dark matter at loop level,” *JHEP* **12** (2018) 089, [arXiv:1810.08139 \[hep-ph\]](#).
 - [9] K. Huitu, N. Koivunen, O. Lebedev, S. Mondal, and T. Toma, “Probing pseudo-Goldstone dark matter at the LHC,” *Phys. Rev. D* **100** (2019) 015009, [arXiv:1812.05952 \[hep-ph\]](#).
 - [10] T. Alanne, M. Heikinheimo, V. Keus, N. Koivunen, and K. Tuominen, “Direct and indirect probes of Goldstone dark matter,” *Phys. Rev. D* **99** (2019) 075028, [arXiv:1812.05996 \[hep-ph\]](#).
 - [11] K. Kannike and M. Raidal, “Phase Transitions and Gravitational Wave Tests of Pseudo-Goldstone Dark Matter in the Softly Broken $U(1)$ Scalar Singlet Model,” *Phys. Rev. D* **99** (2019) 115010, [arXiv:1901.03333 \[hep-ph\]](#).
 - [12] D. Karamitros, “Pseudo Nambu-Goldstone Dark Matter: Examples of Vanishing Direct Detection Cross Section,” *Phys. Rev. D* **99** (2019) 095036, [arXiv:1901.09751 \[hep-ph\]](#).
 - [13] J. M. Cline and T. Toma, “Pseudo-Goldstone dark matter confronts cosmic ray and collider anomalies,” *Phys. Rev. D* **100** (2019) 035023, [arXiv:1906.02175 \[hep-ph\]](#).
 - [14] X.-M. Jiang, C. Cai, Z.-H. Yu, Y.-P. Zeng, and H.-H. Zhang, “Pseudo-Nambu-Goldstone dark matter and two-Higgs-doublet models,” *Phys. Rev. D* **100** (2019) 075011, [arXiv:1907.09684 \[hep-ph\]](#).
 - [15] M. Ruhdorfer, E. Salvioni, and A. Weiler, “A Global View of the Off-Shell Higgs Portal,” *SciPost Phys.* **8** (2020) 027, [arXiv:1910.04170 \[hep-ph\]](#).
 - [16] C. Arina, A. Beniwal, C. Degrande, J. Heisig, and A. Scaffidi, “Global fit of pseudo-Nambu-Goldstone Dark Matter,” *JHEP* **04** (2020) 015, [arXiv:1912.04008 \[hep-ph\]](#).
 - [17] Y. Abe, T. Toma, and K. Tsumura, “Pseudo-Nambu-Goldstone dark matter from gauged $U(1)_{B-L}$ symmetry,” *JHEP* **05** (2020) 057, [arXiv:2001.03954 \[hep-ph\]](#).
 - [18] N. Okada, D. Raut, and Q. Shafi, “Pseudo-Goldstone Dark Matter in gauged $B - L$ extended Standard Model,” [arXiv:2001.05910 \[hep-ph\]](#).
 - [19] S. Glaus, M. Mühlleitner, J. Müller, S. Patel, T. Römer, and R. Santos, “Electroweak Corrections in a Pseudo-Nambu Goldstone Dark Matter Model Revisited,” *JHEP* **12** (2020) 034, [arXiv:2008.12985 \[hep-ph\]](#).

- [20] Y. Abe, T. Toma, and K. Yoshioka, “Non-thermal Production of PNGB Dark Matter and Inflation,” [arXiv:2012.10286 \[hep-ph\]](#).
- [21] Z. Zhang, C. Cai, X.-M. Jiang, Y.-L. Tang, Z.-H. Yu, and H.-H. Zhang, “Phase transition gravitational waves from pseudo-Nambu-Goldstone dark matter and two Higgs doublets,” *JHEP* **05** (2021) 160, [arXiv:2102.01588 \[hep-ph\]](#).
- [22] Y. Abe, T. Toma, K. Tsumura, and N. Yamatsu, “Pseudo-Nambu-Goldstone Dark Matter Model Inspired by Grand Unification,” [arXiv:2104.13523 \[hep-ph\]](#).
- [23] N. Okada, D. Raut, Q. Shafi, and A. Thapa, “Pseudo-Goldstone Dark Matter in $SO(10)$,” [arXiv:2105.03419 \[hep-ph\]](#).
- [24] T. Abe, “The early kinetic decoupling and a pseudo-Nambu Goldstone dark matter model,” [arXiv:2106.01956 \[hep-ph\]](#).
- [25] Y. Abe and T. Toma, “Direct detection of pseudo-Nambu-Goldstone dark matter with light mediator,” *Phys. Lett. B* **822** (2021) 136639, [arXiv:2108.10647 \[hep-ph\]](#).
- [26] T. Biekötter and M. O. Olea-Romacho, “Reconciling Higgs physics and pseudo-Nambu-Goldstone dark matter in the S2HDM using a genetic algorithm,” *JHEP* **10** (2021) 215, [arXiv:2108.10864 \[hep-ph\]](#).
- [27] Y.-P. Zeng, X. Xiao, and W. Wang, “Constraints on Pseudo-Nambu-Goldstone dark matter from direct detection experiment and neutron star reheating temperature,” *Phys. Lett. B* **824** (2022) 136822, [arXiv:2108.11381 \[hep-ph\]](#).
- [28] C. Cai, Y.-P. Zeng, and H.-H. Zhang, “Cancellation mechanism of dark matter direct detection in Higgs-portal and vector-portal models,” *JHEP* **01** (2022) 117, [arXiv:2109.11499 \[hep-ph\]](#).
- [29] R. N. Mohapatra and N. Okada, “Unified model for inflation, pseudo-Goldstone dark matter, neutrino mass, and baryogenesis,” *Phys. Rev. D* **105** (2022) 035024, [arXiv:2112.02069 \[hep-ph\]](#).
- [30] N. Darvishi and B. Grzadkowski, “Pseudo-Goldstone Dark Matter Model with CP violation,” [arXiv:2204.04737 \[hep-ph\]](#).
- [31] T. Abe and Y. Hamada, “A model of pseudo-Nambu-Goldstone dark matter from a softly broken $SU(2)$ global symmetry with a $U(1)$ gauge symmetry,” [arXiv:2205.11919 \[hep-ph\]](#).
- [32] T. Biekötter, P. Gabriel, M. O. Olea-Romacho, and R. Santos, “Direct detection of pseudo-Nambu-Goldstone dark matter in a two Higgs doublet plus singlet extension of the SM,” [arXiv:2207.04973 \[hep-ph\]](#).
- [33] **Particle Data Group** Collaboration, P. A. Zyla *et al.*, “Review of Particle Physics,” *PTEP* **2020** (2020) 083C01.
- [34] Y. Nambu, “Quasiparticles and Gauge Invariance in the Theory of Superconductivity,” *Phys. Rev.* **117** (1960) 648–663.
- [35] J. Goldstone, “Field Theories with Superconductor Solutions,” *Nuovo Cim.* **19** (1961) 154–164.
- [36] K. S. Babu, C. F. Kolda, and J. March-Russell, “Implications of generalized $Z - Z'$ mixing,” *Phys. Rev. D* **57** (1998) 6788–6792, [arXiv:hep-ph/9710441](#).
- [37] J. Lao, C. Cai, Z.-H. Yu, Y.-P. Zeng, and H.-H. Zhang, “Fermionic and scalar dark matter with hidden $U(1)$ gauge interaction and kinetic mixing,” *Phys. Rev. D* **101** (2020) 095031, [arXiv:2003.02516 \[hep-ph\]](#).
- [38] E. J. Chun, J.-C. Park, and S. Scopel, “Dark matter and a new gauge boson through kinetic mixing,” *JHEP* **02** (2011) 100, [arXiv:1011.3300 \[hep-ph\]](#).
- [39] M. T. Frandsen, F. Kahlhoefer, S. Sarkar, and K. Schmidt-Hoberg, “Direct detection of dark matter in models with a light Z' ,” *JHEP* **09** (2011) 128, [arXiv:1107.2118 \[hep-ph\]](#).
- [40] C. P. Burgess, S. Godfrey, H. Konig, D. London, and I. Maksymyk, “Model independent global constraints on new physics,” *Phys. Rev. D* **49** (1994) 6115–6147, [arXiv:hep-ph/9312291](#).

- [41] M. E. Peskin and T. Takeuchi, “A New constraint on a strongly interacting Higgs sector,” *Phys. Rev. Lett.* **65** (1990) 964–967.
- [42] M. E. Peskin and T. Takeuchi, “Estimation of oblique electroweak corrections,” *Phys. Rev. D* **46** (1992) 381–409.
- [43] B. Holdom, “Oblique electroweak corrections and an extra gauge boson,” *Phys. Lett. B* **259** (1991) 329–334.
- [44] **Gfitter Group** Collaboration, M. Baak, J. Cúth, J. Haller, A. Hoecker, R. Kogler, K. Mönig, M. Schott, and J. Stelzer, “The global electroweak fit at NNLO and prospects for the LHC and ILC,” *Eur. Phys. J. C* **74** (2014) 3046, [arXiv:1407.3792 \[hep-ph\]](#).
- [45] Z.-H. Yu, J.-M. Zheng, X.-J. Bi, Z. Li, D.-X. Yao, and H.-H. Zhang, “Constraining the interaction strength between dark matter and visible matter: II. scalar, vector and spin-3/2 dark matter,” *Nucl. Phys. B* **860** (2012) 115–151, [arXiv:1112.6052 \[hep-ph\]](#).
- [46] J. R. Ellis, A. Ferstl, and K. A. Olive, “Reevaluation of the elastic scattering of supersymmetric dark matter,” *Phys. Lett. B* **481** (2000) 304–314, [arXiv:hep-ph/0001005](#).
- [47] **DARWIN** Collaboration, J. Aalbers *et al.*, “DARWIN: towards the ultimate dark matter detector,” *JCAP* **11** (2016) 017, [arXiv:1606.07001 \[astro-ph.IM\]](#).
- [48] M. G. Baring, T. Ghosh, F. S. Queiroz, and K. Sinha, “New Limits on the Dark Matter Lifetime from Dwarf Spheroidal Galaxies using Fermi-LAT,” *Phys. Rev. D* **93** (2016) 103009, [arXiv:1510.00389 \[hep-ph\]](#).
- [49] J. Alwall, R. Frederix, S. Frixione, V. Hirschi, F. Maltoni, O. Mattelaer, H. S. Shao, T. Stelzer, P. Torrielli, and M. Zaro, “The automated computation of tree-level and next-to-leading order differential cross sections, and their matching to parton shower simulations,” *JHEP* **07** (2014) 079, [arXiv:1405.0301 \[hep-ph\]](#).
- [50] A. Alloul, N. D. Christensen, C. Degrande, C. Duhr, and B. Fuks, “FeynRules 2.0 - A complete toolbox for tree-level phenomenology,” *Comput. Phys. Commun.* **185** (2014) 2250–2300, [arXiv:1310.1921 \[hep-ph\]](#).
- [51] J. Bernon and B. Dumont, “Lilith: a tool for constraining new physics from Higgs measurements,” *Eur. Phys. J. C* **75** (2015) 440, [arXiv:1502.04138 \[hep-ph\]](#).
- [52] S. Kraml, T. Q. Loc, D. T. Nhung, and L. D. Ninh, “Constraining new physics from Higgs measurements with Lilith: update to LHC Run 2 results,” *SciPost Phys.* **7** (2019) 052, [arXiv:1908.03952 \[hep-ph\]](#).
- [53] **ATLAS** Collaboration, M. Aaboud *et al.*, “Measurements of Higgs boson properties in the diphoton decay channel with 36 fb^{-1} of pp collision data at $\sqrt{s} = 13\text{ TeV}$ with the ATLAS detector,” *Phys. Rev. D* **98** (2018) 052005, [arXiv:1802.04146 \[hep-ex\]](#).
- [54] **ATLAS** Collaboration, M. Aaboud *et al.*, “Measurement of the Higgs boson coupling properties in the $H \rightarrow ZZ^* \rightarrow 4\ell$ decay channel at $\sqrt{s} = 13\text{ TeV}$ with the ATLAS detector,” *JHEP* **03** (2018) 095, [arXiv:1712.02304 \[hep-ex\]](#).
- [55] **ATLAS** Collaboration, M. Aaboud *et al.*, “Measurements of gluon-gluon fusion and vector-boson fusion Higgs boson production cross-sections in the $H \rightarrow WW^* \rightarrow e\nu\mu\nu$ decay channel in pp collisions at $\sqrt{s} = 13\text{ TeV}$ with the ATLAS detector,” *Phys. Lett. B* **789** (2019) 508–529, [arXiv:1808.09054 \[hep-ex\]](#).
- [56] **CMS** Collaboration, A. M. Sirunyan *et al.*, “Search for invisible decays of a Higgs boson produced through vector boson fusion in proton-proton collisions at $\sqrt{s} = 13\text{ TeV}$,” *Phys. Lett. B* **793** (2019) 520–551, [arXiv:1809.05937 \[hep-ex\]](#).
- [57] **CMS** Collaboration, A. M. Sirunyan *et al.*, “Combined measurements of Higgs boson couplings in proton-proton collisions at $\sqrt{s} = 13\text{ TeV}$,” *Eur. Phys. J. C* **79** (2019) 421, [arXiv:1809.10733](#)

- [hep-ex].
- [58] F. Ambrogio, C. Arina, M. Backovic, J. Heisig, F. Maltoni, L. Mantani, O. Mattelaer, and G. Mohlabeng, “MadDM v.3.0: a Comprehensive Tool for Dark Matter Studies,” *Phys. Dark Univ.* **24** (2019) 100249, [arXiv:1804.00044 \[hep-ph\]](#).
 - [59] **MAGIC, Fermi-LAT** Collaboration, M. L. Ahnen *et al.*, “Limits to Dark Matter Annihilation Cross-Section from a Combined Analysis of MAGIC and Fermi-LAT Observations of Dwarf Satellite Galaxies,” *JCAP* **02** (2016) 039, [arXiv:1601.06590 \[astro-ph.HE\]](#).
 - [60] **Planck** Collaboration, N. Aghanim *et al.*, “Planck 2018 results. VI. Cosmological parameters,” *Astron. Astrophys.* **641** (2020) A6, [arXiv:1807.06209 \[astro-ph.CO\]](#). [Erratum: *Astron. Astrophys.* 652, C4 (2021)].
 - [61] **CEPC Study Group** Collaboration, M. Dong *et al.*, “CEPC Conceptual Design Report: Volume 2 - Physics & Detector,” [arXiv:1811.10545 \[hep-ex\]](#).
 - [62] **FCC** Collaboration, A. Abada *et al.*, “FCC Physics Opportunities: Future Circular Collider Conceptual Design Report Volume 1,” *Eur. Phys. J. C* **79** (2019) 474.
 - [63] H. Baer *et al.*, “The International Linear Collider Technical Design Report - Volume 2: Physics,” [arXiv:1306.6352 \[hep-ph\]](#).
 - [64] K. Griest and D. Seckel, “Three exceptions in the calculation of relic abundances,” *Phys. Rev. D* **43** (1991) 3191–3203.
 - [65] **CMS** Collaboration, A. M. Sirunyan *et al.*, “Search for a new scalar resonance decaying to a pair of Z bosons in proton-proton collisions at $\sqrt{s} = 13$ TeV,” *JHEP* **06** (2018) 127, [arXiv:1804.01939 \[hep-ex\]](#). [Erratum: *JHEP* 03, 128 (2019)].
 - [66] **ATLAS** Collaboration, G. Aad *et al.*, “Search for heavy resonances decaying into a pair of Z bosons in the $\ell^+\ell^-\ell'^+\ell'^-$ and $\ell^+\ell^-\nu\bar{\nu}$ final states using 139 fb^{-1} of proton-proton collisions at $\sqrt{s} = 13$ TeV with the ATLAS detector,” *Eur. Phys. J. C* **81** (2021) 332, [arXiv:2009.14791 \[hep-ex\]](#).
 - [67] **CMS** Collaboration, A. M. Sirunyan *et al.*, “Search for a heavy Higgs boson decaying to a pair of W bosons in proton-proton collisions at $\sqrt{s} = 13$ TeV,” *JHEP* **03** (2020) 034, [arXiv:1912.01594 \[hep-ex\]](#).
 - [68] **ATLAS** Collaboration, “A search for heavy Higgs bosons decaying into vector bosons in same-sign two-lepton final states in pp collisions at $\sqrt{s} = 13$ TeV with the ATLAS detector,” [arXiv:2211.02617 \[hep-ex\]](#).
 - [69] **CMS** Collaboration, A. M. Sirunyan *et al.*, “Search for heavy Higgs bosons decaying to a top quark pair in proton-proton collisions at $\sqrt{s} = 13$ TeV,” *JHEP* **04** (2020) 171, [arXiv:1908.01115 \[hep-ex\]](#). [Erratum: *JHEP* 03, 187 (2022)].
 - [70] **ATLAS** Collaboration, G. Aad *et al.*, “Search for Higgs boson pair production in the two bottom quarks plus two photons final state in pp collisions at $\sqrt{s} = 13$ TeV with the ATLAS detector,” *Phys. Rev. D* **106** (2022) 052001, [arXiv:2112.11876 \[hep-ex\]](#).